

# Room-temperature heralded vibrational state exhibiting sub-Poissonian statistics

Santiago Tarrago Velez,<sup>1</sup> Kilian Seibold,<sup>1</sup> Nils Kipfer,<sup>1</sup> Mitchell D. Anderson,<sup>1</sup> and Christophe Galland<sup>1</sup>

<sup>1</sup>*Institute of Physics, Ecole Polytechnique Fédérale de Lausanne (EPFL), CH-1015 Lausanne, Switzerland*

(Dated: September 5, 2022)

Measurement induced nonlinearity is a powerful tool in quantum optics to prepare non-classical states of light. We apply this concept to prepare a vibrational mode in a non-classical state with sub-Poissonian statistics in a diamond crystal at room temperature, using a scheme that is applicable to any Raman active mode. Upon detection of a single Stokes-shifted photon under pulsed excitation, quantum mechanics predicts that the wave-function describing the correlated vibrational mode collapses into its first excited energy eigenstate (Fock state  $n = 1$ ). We prove this by mapping the vibrational state onto an anti-Stokes photon, on which we perform a Hanbury-Brown and Twiss intensity interference measurement. Our data reveals deep sub-Poissonian statistics conditioned on the success of the Stokes measurement, and provides the first demonstration of this effect with a mechanical vibration in ambient conditions. Our work is also a proof-of-principle demonstration of a broadly tunable heralded single photon source with integrated short-lived quantum memory.

## I. INTRODUCTION

Photon statistics, and in particular second order intensity correlation functions, have been critical to the development of quantum optics, starting with the first intensity correlation experiments performed by Hanbury-Brown and Twiss from thermal sources [1]. The subsequent developments in our understanding of first- and second-order coherence of light [2, 3] form the basis of most experimental measures of the non-classicality of a light field.

Much more recently, researchers have turned their efforts to revealing non-classical behavior in mechanical oscillators. A harmonic mechanical oscillator is described by the same mathematical operator as a mode of the light field. However, its oscillation frequency  $\Omega_m$  is usually much smaller than the environment temperature  $T_0$ , making thermal noise overwhelmingly stronger than quantum noise ( $k_B T_0 \gg \hbar \Omega_m$ ). Revealing quantum effects via precise quadrature measurements [4, 5] or single photon detection [6–8] on the mechanical sidebands generated by the interaction of micro-fabricated oscillators with a laser beam remains a challenging task. Despite these difficulties, the prospect of harnessing mechanical oscillators coupled to light as quantum-coherent nonlinear elements [9–11] and quantum memories [12–15] is a strong drive to investigate optomechanical systems in the quantum regime.

Here, we show that a fundamental signature of non-classicality, namely sub-Poissonian statistics, can be observed at room temperature in high-frequency vibrational modes. Since diamond, with its Raman active phonon mode at 39.9 THz, has been used recently to demonstrate quantum information processing protocols and quantum memories [16–21], we use this crystal in a proof-of-principle experiment. Contrary to previous experiments [16–21] our scheme does not depend on the polarization selection rules associated with a specific Raman transition and crystal orientation; it is generally applicable to Raman-active vibrational modes, opening un-

limited opportunities to study other crystals and molecular systems.

Under laser excitation of a non-resonant Raman transition with a pulse of duration short compared to the vibrational lifetime (but long compared to the vibrational period), a two-mode squeezed state is generated (Fig. 1), exhibiting perfect number correlations between the vibrational and Stokes modes. Following the approach used to generate heralded single photons in quantum optics [22], we first probabilistically prepare the vibrational mode in a state close to the first excited energy eigenstate (Fock state  $|n = 1\rangle$ ) through projective single-photon measurement on a propagating Stokes mode [14]. After a variable delay, the state of the vibrational mode is subsequently mapped onto the state of an anti-Stokes photon thanks to a second laser pulse centered at a different wavelength [6, 14]. Second order intensity correlations are measured on the anti-Stokes photons, revealing the statistics of the vibrational state. Conditional on the Stokes detection event, the normalized second-order moment drops from  $g^{(2)}(0) \approx 2$  (thermal statistics) down to  $g^{(2)}(0) < 0.1$ . This sub-poissonian vibrational statistics persists for several picoseconds after the preparation pulse, decaying with the characteristic lifetime of the vibrational mode ( $\tau_{vib} \approx 3.9$  ps). Our experiment constitutes an implementation of the DLCZ scheme [23] on a vibrational mode at room temperature, which forms the basis for on-demand single photon sources [24–26], entanglement creation between two systems [27–29] and its remote distribution by entanglement swapping [30], provided that systems with longer vibrational coherence times are used.

## II. THEORETICAL DESCRIPTION

A Hamiltonian describing the nonlinear Raman interaction can be written as [31]

$$H_I^{w(r)} = i\hbar g_S^{w(r)} \hat{a}_S^{w(r)\dagger} \hat{b}^\dagger + i\hbar g_{aS}^{w(r)} \hat{a}_{aS}^{w(r)\dagger} \hat{b} + h.c. \quad (1)$$

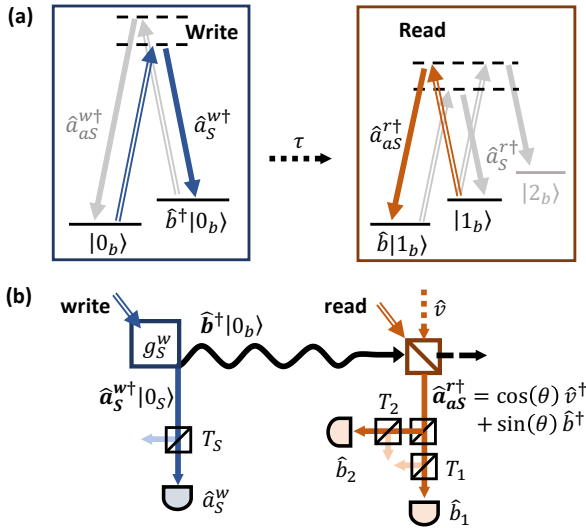


FIG. 1: Conceptual scheme of the experiment. (a) Energy diagram of the Raman transitions involved in the write and read steps. The light grey arrows correspond to the terms of eq. (1) for which emitted photons are not detected. (b) Diagram showing the optical and vibrational modes. Beam splitters are used to model the read interaction (mixing angle  $\theta$ ) and the losses (overall detection efficiency =  $T_{S,1,2}$ ).

where we defined the Stokes  $\hat{a}_S^{w(r)\dagger}$  and anti-Stokes  $\hat{a}_{as}^{w(r)\dagger}$  creation operators. The superscripts stand for the write ( $w$ ) and read ( $r$ ) pulses. Experimentally, each mode has the temporal envelop of the mode-locked laser pulses and the spatial profile of the single-mode fiber used in detection. They are all centered at different wavelengths with negligible spectral overlap. Due to the conservation of energy and momentum in the Raman scattering process, a single spatio-temporal mode of the vibration is involved, with the creation operator  $\hat{b}^\dagger$ . The coupling rates  $g_S^{w(r)}$  and  $g_{as}^{w(r)}$  are complex numbers proportional to the write (read) pump amplitude and the Raman cross-section of the vibrational mode.

The Hamiltonian is similar to the one describing Raman transitions in atomic ensembles [23] and in linearized cavity optomechanics [32], but in those systems the presence of electronic transitions or optical cavities implies that only one term of the Hamiltonian is resonant. Typically, the Stokes interaction is resonant during the write pulse, while the anti-Stokes part is resonant during the read pulse, and the non-resonant terms can be neglected in the rotating wave approximation. Although there is no nearby resonance in our experiment (the band gap of diamond is 5.47 eV), all essential results of our measurements can be described by taking only one term into account for each step, due to the post-selection procedure.

This neglects higher order interactions, in particular the creation of correlated Stokes – anti-Stokes pairs during a single pulse (write or read) [31, 33–36], an effective four-wave mixing process involving two degenerate pump

photons. This higher-order term gives rise to an additional noise on the detector, whose effect on the measurement is similar to that of dark counts. While this noise is completely negligible compared to the Stokes signal, the anti-Stokes detection rate is significantly lower than the Stokes rate so that this noise cannot be neglected in the read step for the highest pump powers. The quantum model used in Fig. 4 includes this term explicitly in the Hamiltonian, while it is taken into account empirically (it is contained into the dark count probability given as input) in the simpler model used to fit Fig. 3.

### A. Readout stage

For clarity, we will first comment on the readout procedure (Fig. 1). The Hamiltonian governing the dynamics of the anti-Stokes mode being detected is  $H_I^r = i\hbar g_{as}^{r\dagger} \hat{a}_{as}^r \hat{b} + h.c.$  and it represents a beam splitter interaction between the anti-Stokes and vibrational modes. We can express the input-output relation as  $\hat{a}_{as}^r = \cos(\theta)\hat{v}^\dagger + \sin(\theta)\hat{b}^\dagger$  with the mixing angle  $\theta = g_{as}^r \Delta T$  for the simplified case of a constant interaction during a pulse duration  $\Delta T$  (the numerical simulations shown in Fig. 4 account for the Gaussian shape of the pulse). The mode  $v$  describing the anti-Stokes input mode (before the read pulse) is in the vacuum state, yielding

$$\langle : (\hat{a}_{as}^{r\dagger} \hat{a}_{as}^r) ^n : \rangle = \sin^2(\theta) \langle : (\hat{b}^\dagger \hat{b}) ^n : \rangle \quad (2)$$

for any integer  $n \geq 1$ , where  $::$  denotes normal ordering. Eq. (2) expresses the fact that photon counting (and more generally direct intensity measurement) is insensitive to vacuum noise. As a result, normalized moments measured on the anti-Stokes mode are faithfully mapping the statistics of the vibrational mode, independently of the efficiency of the readout process (as long as added noise can be neglected).

### B. Write stage

We now turn to the dynamics of the Stokes mode during the write pulse, governed by  $H_I^w = i\hbar g_S^{w\dagger} \hat{a}_S^{w\dagger} \hat{b}^\dagger + h.c.$ , which has the form of a two-mode squeezing interaction and leads to the creation of maximally correlated pairs of vibrational excitations  $\hat{b}^\dagger |vac\rangle$  and Stokes photons  $\hat{a}_S^{w\dagger} |vac\rangle$ . When both modes are initially in the vacuum state  $|vac\rangle$ , the final state after the write pulse is [37, 38]

$$|\Psi\rangle_{S,b} = \sqrt{1-p} \sum_{n=0}^{\infty} \sqrt{p^n} |n, n\rangle_{S,b} \quad (3)$$

where  $|n, n\rangle_{S,b} \equiv \frac{(\hat{b}^\dagger \hat{a}_S^{w\dagger})^n}{n!} |vac\rangle$ . For the simplified situation of a constant interaction switched on during  $\Delta t$  we have  $\sqrt{p} = \tanh(g_S^w \Delta t)$ . The pair-wise correlation,

which violates the Cauchy-Schwarz inequality [39], can be revealed by a coincidence measurement between Stokes and anti-Stokes:  $g_{S,aS}^{(2)} = \frac{\langle \hat{b}^\dagger \hat{a}_S^{\dagger w} \hat{a}_S^w \hat{b} \rangle}{\langle \hat{b}^\dagger \hat{b} \rangle \langle \hat{a}_S^{\dagger w} \hat{a}_S^w \rangle} = 1 + \frac{1}{p} \gg 1$  for  $p \ll 1$  (Figs. 3a and 4a).

Conditional on the detection of at least one photon in the Stokes mode, the post-measurement state is obtained as

$$\hat{\rho}_b^{cond} = \frac{1-p}{p} \sum_{n=1}^{\infty} p^n |n\rangle_b \langle n| \approx |1\rangle \langle 1| + p |2\rangle \langle 2| \quad (4)$$

where the last approximation is valid when  $p \ll 1$ .

### C. Heralded statistics of the two-mode squeezed state

As mentioned above, normalized correlation functions measured on the anti-Stokes mode are equal to those that would be measured directly on the vibrational mode. The normalized intensity correlation of the vibrational mode, conditional on the detection of a photon in mode  $a_S$  is

$$\begin{aligned} g_{Cond}^{(2)}(\tau) &= \frac{\langle \hat{b}^{\dagger(\tau)} \hat{b}^{\dagger(\tau)} \hat{b}^{(\tau)} \hat{b}^{(\tau)} \rangle_{Cond}}{\langle \hat{b}^{\dagger(\tau)} \hat{b}^{(\tau)} \rangle_{Cond}^2} \\ &= \frac{\langle \hat{b}_2^{\dagger(\tau)} \hat{b}_1^{\dagger(\tau)} \hat{b}_1^{(\tau)} \hat{b}_2^{(\tau)} \rangle_{Cond}}{\langle \hat{b}_1^{\dagger(\tau)} \hat{b}_1^{(\tau)} \rangle_{Cond} \langle \hat{b}_2^{\dagger(\tau)} \hat{b}_2^{(\tau)} \rangle_{Cond}} \quad (5) \end{aligned}$$

where  $\langle \cdot \rangle_{Cond}$  indicates the expectation value taken on the post-measurement state after detecting the heralding Stokes photon, and  $\tau$  is the time delay since the herald detection event [56]. The modes  $b_1$  and  $b_2$  are obtained by splitting the anti-Stokes signal on two detectors, see Fig. 1b.

Since the expectation value of an operator  $\hat{X}$  after a photon number measurement on mode  $a_S$  is  $\langle \hat{X} \rangle = \frac{\langle \hat{a}_S^\dagger \hat{X} \hat{a}_S \rangle}{\langle \hat{a}_S^\dagger \hat{a}_S \rangle}$  [40] we can rewrite Eq. (5) as

$$g_{Cond}^{(2)}(\tau) = \frac{\langle \hat{a}_S^{\dagger(0)} \hat{b}_2^{\dagger(\tau)} \hat{b}_1^{\dagger(\tau)} \hat{b}_1^{(\tau)} \hat{b}_2^{(\tau)} \hat{a}_S^{(0)} \rangle \langle \hat{a}_S^{\dagger(0)} \hat{a}_S^{(0)} \rangle}{\langle \hat{a}_S^{\dagger(0)} \hat{b}_1^{\dagger(\tau)} \hat{b}_1^{(\tau)} \hat{a}_S^{(0)} \rangle \langle \hat{a}_S^{\dagger(0)} \hat{b}_2^{\dagger(\tau)} \hat{b}_2^{(\tau)} \hat{a}_S^{(0)} \rangle} \quad (6)$$

In the limit of small  $p$ , explicit evaluation of eq. (6) on the state  $|\Psi\rangle_{S,b}$  of eq. (3) yields

$$g_{Cond}^{(2)} \simeq \frac{4P(2,2)}{P(1,1)} = 4p \quad (7)$$

where  $P(n,n)$  denotes the probability that  $n$  pairs were generated. In our experiment, and following the pioneering work of Grangier *et al* [22], we evaluate the parameter

$$\alpha = \frac{N_{b_1, b_2, a_S} N_{a_S}}{N_{b_1, a_S} N_{b_2, a_S}} \quad (8)$$

where  $N_{b_1, b_2, a_S}$  is the number of events where photons were detected simultaneously in modes  $b_1$ ,  $b_2$  and  $a_S$

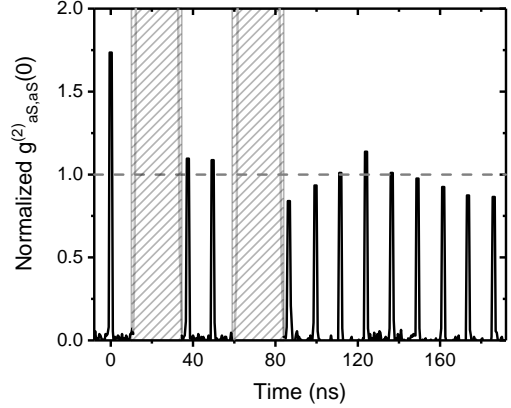


FIG. 2: Coincidence histogram between detectors  $b_1$  and  $b_2$  of Fig. 1 without the write pulse, probing the equilibrium state of the vibrational mode. The counts in the shaded regions (not shown) are due to cross-talk between the two detectors, when the detection avalanche emits a photon that is scattered onto the other detector. The ratio of counts in the central peak to the average counts in the side peaks (dashed line) gives a value of  $g_{b_1, b_2}^{(2)}(0) = g_{a_S, a_S}^{(2)}(0) = 1.73 \pm 0.11$ , compatible with the single-mode thermal statistics once accounting for some background noise.

(triple coincidence),  $N_{b_1(b_2), a_S}$  the number of two-fold coincidences and  $N_{a_S}$  the number of  $a_S$  detection events.

It is important to note that  $\alpha$  does not necessarily give the same result as  $g_{Cond}^{(2)}$ . More precisely, if the detection efficiency of the herald mode  $a_S$  is  $0 < T_S \leq 1$  (which we model as a beam splitter with transmittance  $T_S$  placed before the detector, see Fig. 1b) we find

$$\alpha \simeq (4 - 2T_S) \frac{P(2,2)}{P(1,1)} = (4 - 2T_S)p \quad (9)$$

which recovers the result of eq. (7) only in the limit of low efficiency. However, for 100% herald detection efficiency ( $T_S = 1$ ) then  $\alpha = \frac{1}{2}g_{Cond}^{(2)}$ . A more complete model for detection [41] confirms this result when the dark count probability is small compared to  $p \times T_S$ . The case of non-conditional antibunching measurements was discussed e.g. in [42].

## III. EXPERIMENTAL REALIZATION

### A. Setup and measurement procedure

Our experimental setup is a slightly modified version of that presented in [39]. Two synchronized laser pulse trains at 810 nm and 695 nm of duration  $\Delta t \approx 100$  fs are produced by a Ti:Sapph oscillator (Tsunami, Spectra Physics, 80 MHz repetition rate) and a frequency-doubled optical parametric oscillator (OPO-X fs, APE Berlin), respectively. The write pulses are provided by

the OPO, while the Ti:Sapph provides the read pulses, which are passed through a delay line before being overlapped with the OPO on a dichroic mirror. The sample is a synthetic diamond crystal ( $\sim 300 \mu\text{m}$  thick, from Lake-Diamond) cut along the 1-0-0 crystal axis and is probed in transmission using two microscope objectives (numerical aperture 0.8 and 0.9). The laser light is blocked using long-pass and short-pass tunable interference filters (Semrock), leaving only a window for the Stokes signal from the write pulse and the anti-Stokes signal from the read pulse. After being collected in a single mode fiber for spatial mode filtering and recollimated, these two signals are separated with a tunable long-pass filter used as a dichroic mirror. After an additional band-pass filter each signal is coupled into a multi-mode fiber, where the Stokes photons are sent into a single photon avalanche photo-diode (SPAD), and the anti-Stokes photons are sent through a 50-50 splitting ratio multi-mode fiber and into two SPADs. The three SPADs are then connected into a coincidence counter (PicoQuant TimeHarp 260).

We save the time tags of the events where a click in one of the anti-Stokes channels was preceded by a click in the Stokes channel. This allows us to find the events where the three channels clicked simultaneously (within the same laser repetition), as well as to build a delay histogram using the Stokes channel as the start and either of the anti-Stokes channels as the stop.

The normalized Stokes-anti-Stokes correlation  $g_{S,aS}^{(2)}(\tau)$  is derived from the coincidence histogram as the ratio of the number of coincidences in a same pulse sequence over the average number of accidentals (side peaks in Fig. 2) where detector clicks come from different pulse sequences spaced by 12.5 ns. Our overall detection efficiency is estimated to be between 5% and 15 so that the measured parameter  $\alpha$  satisfies  $\alpha(\tau) \approx g_{C\text{ond}}^{(2)}(\tau)$  according to eq. (9).

## B. Results

In the absence of a preparation step, the anti-Stokes signal should carry the thermal statistics of the vibrational mode. To check this, we measured the unconditional second order correlation of the anti-Stokes mode (in the absence of any write pulse), obtaining  $g_{aS,aS}^{(2)} = 1.73 \pm 0.11$ , as shown in Fig. 2. This value is slightly lower than the expected value of 2 for a single mode thermal state, but higher than the value  $1 + \frac{1}{N}$  for a thermal state of  $N > 1$  modes. We attribute this discrepancy to the noise in the anti-Stokes channel coming from degenerate four-wave mixing in the sample (which includes the second-order Stokes-anti-Stokes process [31] discussed above). In fact, we measured  $g_{S,S}^{(2)} = 2.0 \pm 0.1$  on the Stokes mode [39], as expected for the marginal statistics in the two-mode squeezed state when a single pair of mode is involved [41], confirming that our experiment is truly probing a single vibrational mode.

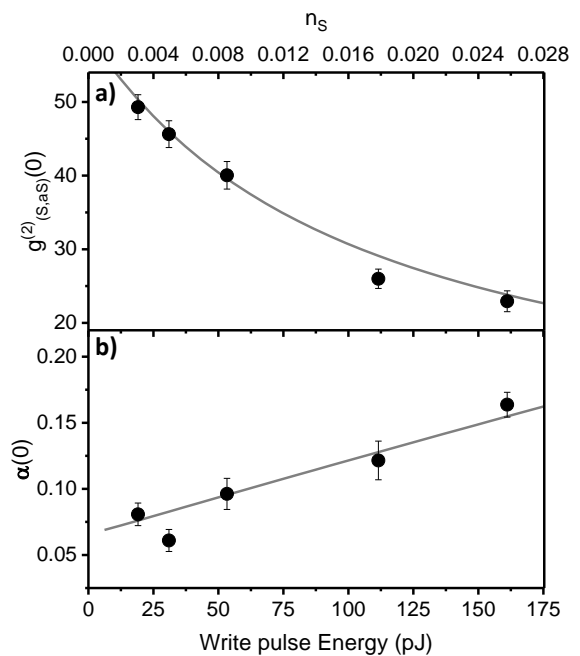


FIG. 3: Dependence on the write laser power of (a) normalized Stokes-anti-Stokes correlations and (b) the heralded vibrational statistics (represented by the parameter  $\alpha(0)$ ), both taken at zero write-read delay (full circles). Statistical error bars are obtained from the square root of the total number of events. The fitting curves (solid lines) are derived from the model of Ref. [41] adapted for our experiment as described in [39]. The detection efficiency (10 %) and relative efficiency of the read process compared to the write process (30 %) were adjusted manually to obtain the best fits (two common parameters, fixed for both fits), yielding values consistent with experimental expectations.

In contrast, when we measure the statistics of the heralded vibrational state conditional on Stokes detection, we find that  $\alpha < 1$ , evidencing sub-Poissonian statistics, as shown in Fig. 3b. As we increase the power,  $\alpha$  increases from  $0.06 \pm 0.01$  to  $0.16 \pm 0.01$ , while the Stokes-anti-Stokes correlation  $g_{S,aS}^{(2)(0)}$  decreases from  $49 \pm 2$  to  $23 \pm 1$ . These trends are due to the increasing probability of exciting two or more vibrational quanta, and are well reproduced by a model adapted from Ref. [41] taking into account the estimated detection efficiency and the measured detector dark count rates (see the Supplementary Material of [39], Section 2, for details). This proves that our experiment can be faithfully modeled using the Hamiltonian (1) and considering only the two-mode squeezing interaction in the write step and the beam-splitter interaction in the read step.

We then investigate the temporal dynamics of the heralded vibrational state by changing the delay between the write and read pulses, Fig. 4. When the pulses overlap in time we measure  $g_{S,aS}^{(2)}(0) = 33.5 \pm 1.3$  and  $\alpha(0) = 0.11 \pm 0.01$ . The second order cross-correlation be-

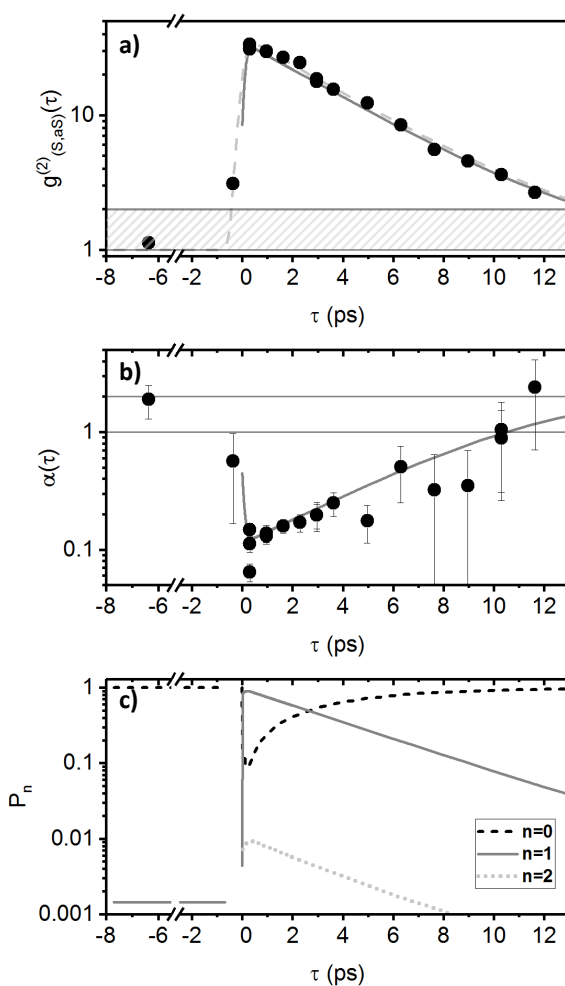


FIG. 4: (a) Experimentally measured (full circles) dependence on the write-read time delay of the (a) normalized Stokes-anti-Stokes correlations and (b) the heralded vibrational statistics (represented by the parameter  $\alpha(\tau)$ ) together with the numerical evaluation of the open quantum system master equation (solid lines) (see SM of [39], Sec. 3, for details on the model). Statistical error bars are obtained from the square root of the total number of events. The quantum model requires a free parameter for the vibrational dissipation rate that can be obtained from an exponential fit to the data of panel (a) (dashed line), yielding a vibrational lifetime  $\tau_{vib} = 3.9 \pm 0.3$  ps. (c) Occupation probability  $P_n$  of the number states with  $n$  excitations in the conditional vibrational state, inferred from the quantum model used to fit panel (a) and (b). At negative delay, the lines represent the thermal vibrational occupancy, with  $\langle \hat{b}^\dagger \hat{b} \rangle_{th} \approx 1.4 \cdot 10^{-3}$ .

tween Stokes and anti-Stokes decays exponentially with a time constant of  $\tau = 3.9 \pm 0.3$  ps (bounds for 95% confidence), consistent with [39]. The behavior of  $\alpha$ , measured here for the first time on a vibrational mode at room temperature, perfectly mirrors this evolution, starting at  $\alpha(\tau < 0) = 1.9 \pm 0.6$  at negative delays (thermal state), dropping to  $\alpha(0) = 0.11 \pm 0.01$  at zero delay,

and then returning toward thermal equilibrium as the prepared vibrational Fock state thermalizes with its environment. The larger uncertainty in the data at long and at negative delays is due to the reduced rate of coincidences, because of the very small mean thermal occupancy  $\langle \hat{b}^\dagger \hat{b} \rangle_{th} \approx 1.4 \cdot 10^{-3}$  of the vibrational mode. In Fig. 4(b) we show three measurements for  $\alpha(0)$  which were taken under the same conditions, but during three different days, to illustrate the systematic uncertainty on the results. These are mainly due to power and alignment fluctuations.

Finally, we numerically solve the time-dependent quantum master equation of the open system in the Lindbladian form with the Hamiltonian (1), as described in the Supplementary Material of [39], Section 3, with only two adjustable parameters:

- The vibrational decay rate  $\tau = 3.9 \pm 0.3$  ps, which is extracted from an exponential fit to Fig. 4(a)
- The amount of noise on the anti-Stokes detectors, which is modeled as a thermal occupancy of the anti-Stokes mode proportional to the square of the instantaneous laser power in the read pulse. As explained in [39], this is experimentally justified by the observation of a broadband four-wave mixing background. Note that Stokes-anti-Stokes pair creation during a single read pulse [31] is contained in the full Hamiltonian (1) and also generates noise proportional to the square of the laser intensity.

Using a value for the noise that is consistent with our experimental estimates, we are able to reproduce quantitatively the time dependence of the Stokes-anti-Stokes correlation and the conditional state statistics  $\alpha(\tau)$ . Interestingly, from the model we can extract the number distribution  $P_n$  in the conditional vibrational state, i.e. the probability to find the vibrational mode in the  $n^{\text{th}}$  excited state, conditional on the click of the Stokes detector. Its evolution as a function of the write-read delay  $\tau$  is plotted in Fig. 4(c). Noteworthy is the high purity of the conditional vibrational state with respect to the Fock state  $|n=1\rangle_b$ , since its normalized second order correlation is  $\frac{2P_2}{P_1^2} \approx 0.02$ . This is much lower than the measured parameter  $\alpha \approx 0.1$  (because the background noise impinging on the anti-Stokes detectors affects  $\alpha$ ) and highlights the potential of the technique to produce high-purity single photon states provided that the contribution of other non-linearities is mitigated, for example by engineering the local density of states of the electromagnetic field around the vibrational mode [52].

#### IV. CONCLUSION

We have demonstrated for the first time that a high-frequency Raman active vibrational mode can be prepared, at room temperature, in a state featuring sub-Poissonian statistics, conditional on the detection of a

Stokes photon. This research opens the door to the study of quantum effects in the vibrational dynamics of many other Raman-active modes, in immobilized molecules [43], liquids, gases [44–46] and solid-state systems. The dynamics of the higher excited Fock state could be probed by conditioning on the detection of 2 Stokes photons, and compared with the measurement made on electromagnetic modes in superconducting circuits [47] and optical cavities [48]. Finally, our results have direct implications for the development of quantum technologies. Our scheme shows that vibrational modes at room temperature can be used as quantum memories in the DLCZ scheme [23], but their coherence time would need to be significantly increased to enable long distance entanglement distribution. One track of investigation is to use molecular species in the liquid [49] or gas [44–46] phases, where longer vibrational lifetimes have been observed, but research is needed to extend their coherence times

[50, 51]. Moreover, our results show that heralded single photons can be produced with an arbitrary choice of the herald and signal wavelengths and bandwidth, using the vibrational mode as short term memory, extending the reach of recent experiments [20]. Here, the challenge is to increase the readout efficiency, possibly using small-mode volume optical or plasmonic cavities [52, 53], or resonant Raman scattering [54, 55]. If successful, this would also realize a quantum coherent interface for frequency conversion at the single photon level.

## V. ACKNOWLEDGEMENTS

Funding for this research was provided by the Swiss National Science Foundation, grant number PP00P2-170684.

---

[1] R. H. Brown and R. Q. Twiss, *Nature* **177**, 27 (1956).

[2] R. J. Glauber, *Phys. Rev.* **131**, 2766 (1963).

[3] R. J. Glauber, *Phys. Rev.* **130**, 2529 (1963).

[4] T. P. Purdy, K. E. Grutter, K. Srinivasan, and J. M. Taylor, *Science* **356**, 1265 (2017).

[5] V. Sudhir, R. Schilling, S. A. Fedorov, H. Schütz, D. J. Wilson, and T. J. Kippenberg, *Phys. Rev. X* **7**, 031055 (2017).

[6] R. Riedinger, S. Hong, R. A. Norte, J. A. Slater, J. Shang, A. G. Krause, V. Anant, M. Aspelmeyer, and S. Gröblacher, *Nature* **530**, 313 (2016).

[7] S. Hong, R. Riedinger, I. Marinković, A. Wallucks, S. G. Hofer, R. A. Norte, M. Aspelmeyer, and S. Gröblacher, *Science* **358**, 203 (2017).

[8] R. Riedinger, A. Wallucks, I. Marinkovic, C. Löschnauer, M. Aspelmeyer, S. Hong, and S. Gröblacher, ArXiv171011147 Cond-Mat Physics-physics Physicsquant-Ph (2017).

[9] K. Stannigel, P. Komar, S. J. M. Habraken, S. D. Bennett, M. D. Lukin, P. Zoller, and P. Rabl, *Phys Rev Lett* **109**, 013603 (2012).

[10] M. Ludwig, A. H. Safavi-Naeini, O. Painter, and F. Marquardt, *Phys Rev Lett* **109**, 063601 (2012).

[11] P. Kómár, S. D. Bennett, K. Stannigel, S. J. M. Habraken, P. Rabl, P. Zoller, and M. D. Lukin, *Phys. Rev. A* **87**, 013839 (2013).

[12] A. H. Safavi-Naeini, T. P. M. Alegre, J. Chan, M. Eichenfield, M. Winger, Q. Lin, J. T. Hill, D. E. Chang, and O. Painter, *Nature* **472**, 69 (04 2011/04/07/print).

[13] D. E. Chang, A. H. Safavi-Naeini, M. Hafezi, and O. Painter, *New J. Phys.* **13**, 023003 (2011).

[14] C. Galland, N. Sangouard, N. Piro, N. Gisin, and T. J. Kippenberg, *Phys Rev Lett* **112**, 143602 (2014).

[15] R. Y. Teh, S. Kiesewetter, M. D. Reid, and P. D. Drummond, *Phys. Rev. A* **96**, 013854 (2017).

[16] K. C. Lee, B. J. Sussman, M. R. Sprague, P. Michelberger, K. F. Reim, J. Nunn, N. K. Langford, P. J. Bustard, D. Jaksch, and I. A. Walmsley, *Nat Photon* **6**, 41 (2012).

[17] D. G. England, P. J. Bustard, J. Nunn, R. Lausten, and B. J. Sussman, *Phys. Rev. Lett.* **111**, 243601 (2013).

[18] D. G. England, K. Fisher, J.-P. W. MacLean, P. J. Bustard, R. Lausten, K. J. Resch, and B. J. Sussman, *Phys. Rev. Lett.* **114**, 053602 (2015).

[19] P.-Y. Hou, Y.-Y. Huang, X.-X. Yuan, X.-Y. Chang, C. Zu, L. He, and L.-M. Duan, *Nat. Commun.* **7**, 11736 (2016).

[20] K. A. G. Fisher, D. G. England, J.-P. W. MacLean, P. J. Bustard, K. J. Resch, and B. J. Sussman, *Nat. Commun.* **7**, 11200 (2016).

[21] K. A. G. Fisher, D. G. England, J.-P. W. MacLean, P. J. Bustard, K. Heshami, K. J. Resch, and B. J. Sussman, *Phys. Rev. A* **96**, 012324 (2017).

[22] P. Grangier, G. Roger, and A. Aspect, *EPL* **1**, 173 (1986).

[23] L. M. Duan, M. D. Lukin, J. I. Cirac, and P. Zoller, *Nature* **414**, 413 (11 2001/11/22/print).

[24] C. W. Chou, S. V. Polyakov, A. Kuzmich, and H. J. Kimble, *Phys. Rev. Lett.* **92**, 213601 (2004).

[25] S. Chen, Y.-A. Chen, T. Strassel, Z.-S. Yuan, B. Zhao, J. Schmiedmayer, and J.-W. Pan, *Phys Rev Lett* **97**, 173004 (2006).

[26] D. N. Matsukevich, T. Chanelière, S. D. Jenkins, S.-Y. Lan, T. A. B. Kennedy, and A. Kuzmich, *Phys Rev Lett* **97**, 013601 (2006).

[27] C. W. Chou, H. de Riedmatten, D. Felinto, S. V. Polyakov, S. J. van Enk, and H. J. Kimble, *Nature* **438**, 828 (2005).

[28] D. N. Matsukevich, T. Chanelière, S. D. Jenkins, S.-Y. Lan, T. A. B. Kennedy, and A. Kuzmich, *Phys. Rev. Lett.* **96**, 030405 (2006).

[29] J. Laurat, K. S. Choi, H. Deng, C. W. Chou, and H. J. Kimble, *Phys. Rev. Lett.* **99**, 180504 (2007).

[30] C.-W. Chou, J. Laurat, H. Deng, K. S. Choi, H. de Riedmatten, D. Felinto, and H. J. Kimble, *Science* **316**, 1316 (2007).

[31] C. A. Parra-Murillo, M. F. Santos, C. H. Monken, and A. Jorio, *Phys. Rev. B* **93**, 125141 (2016).

[32] M. Aspelmeyer, T. J. Kippenberg, and F. Marquardt, *Rev. Mod. Phys.* **86**, 1391 (2014).

[33] M. K. Schmidt, R. Esteban, A. González-Tudela,

G. Giedke, and J. Aizpurua, ACS Nano **10**, 6291 (2016).

[34] M. Kasperczyk, A. Jorio, E. Neu, P. Maletinsky, and L. Novotny, Opt. Lett. **40**, 2393 (2015).

[35] M. Kasperczyk, F. S. de Aguiar Júnior, C. Rabelo, A. Saraiva, M. F. Santos, L. Novotny, and A. Jorio, Phys. Rev. Lett. **117**, 243603 (2016).

[36] A. Saraiva, F. S. d. A. Júnior, R. de Melo e Souza, A. P. Pena, C. H. Monken, M. F. Santos, B. Koiller, and A. Jorio, Phys. Rev. Lett. **119**, 193603 (2017).

[37] L. Mandel and E. Wolf, *Optical Coherence and Quantum Optics* (Cambridge University Press, 1995).

[38] D. F. Walls and G. J. Milburn, *Quantum Optics* (Springer-Verlag, Berlin Heidelberg, 2008), 2nd ed., ISBN 978-3-540-28573-1.

[39] M. D. Anderson, S. Tarrago Velez, K. Seibold, H. Flayac, V. Savona, N. Sangouard, and C. Galland, Phys. Rev. Lett. **120**, 233601 (2018).

[40] M. Razavi, I. Söllner, E. Bocquillon, C. Couteau, R. Laflamme, and G. Weihs, J. Phys. B At. Mol. Opt. Phys. **42**, 114013 (2009).

[41] P. Sekatski, N. Sangouard, F. Bussieres, C. Clausen, N. Gisin, and H. Zbinden, J. Phys. B At. Mol. Opt. Phys. **45**, 124016 (2012).

[42] M. J. Stevens, S. Glancy, S. W. Nam, and R. P. Mirin, Opt. Express, OE **22**, 3244 (2014).

[43] S. Yampolsky, D. A. Fishman, S. Dey, E. Hulkko, M. Banik, E. O. Potma, and V. A. Apkarian, Nat Photon **8**, 650 (2014).

[44] P. J. Bustard, R. Lausten, D. G. England, and B. J. Sussman, Phys. Rev. Lett. **111**, 083901 (2013).

[45] P. J. Bustard, J. Erskine, D. G. England, J. Nunn, P. Hockett, R. Lausten, M. Spanner, and B. J. Sussman, Opt. Lett., OL **40**, 922 (2015).

[46] P. J. Bustard, D. G. England, K. Heshami, C. Kupchak, and B. J. Sussman, Opt. Lett., OL **41**, 5055 (2016).

[47] H. Wang, M. Hofheinz, M. Ansmann, R. C. Bialczak, E. Lucero, M. Neeley, A. D. O'Connell, D. Sank, J. Wenner, A. N. Cleland, et al., Phys. Rev. Lett. **101**, 240401 (2008).

[48] M. Brune, J. Bernu, C. Guerlin, S. Deléglise, C. Sayrin, S. Gleyzes, S. Kuhr, I. Dotsenko, J. M. Raimond, and S. Haroche, Phys. Rev. Lett. **101**, 240402 (2008).

[49] S. R. J. Brueck and R. M. Osgood, Chemical Physics Letters **39**, 568 (1976).

[50] S. F. Fischer and A. Laubereau, Chemical Physics Letters **35**, 6 (1975).

[51] M. Gruebele, J. Phys.: Condens. Matter **16**, R1057 (2004).

[52] P. Roelli, C. Galland, N. Piro, and T. J. Kippenberg, Nat Nano **11**, 164 (2016).

[53] F. Benz, M. K. Schmidt, A. Dreismann, R. Chikkaraddy, Y. Zhang, A. Demetriadou, C. Carnegie, H. Ohadi, B. de Nijs, R. Esteban, et al., Science **354**, 726 (2016).

[54] A. Jorio, M. Kasperczyk, N. Clark, E. Neu, P. Maletinsky, A. Vijayaraghavan, and L. Novotny, Nano Lett. **14**, 5687 (2014).

[55] T. Jiang, H. Hong, C. Liu, W.-T. Liu, K. Liu, and S. Wu, Nano Lett. (2018).

[56] Note that the time delay  $\tau$  used here is not the delay between the two operators  $\hat{b}_1$  and  $\hat{b}_2$  as is in the usual definition.